Synthesis, characterization, and photocleavage of *bis*-decyl pteroic acid: A folate derivative with affinity to biomembranes

José Luis Fonseca[1], M. José Sosa[1], Gabriela Petroselli[2], Rosa Erra-Balsells[2], Matías I. Quindt[2], Sergio M. Bonesi[2], Alexander Greer[3,4], Edyta M. Greer[5], Andrés H. Thomas[1], Mariana Vignoni[1*]

[1] Departamento de Química, Facultad de Ciencias Exactas, Instituto de Investigaciones Fisicoquímicas Teóricas y Aplicadas (INIFTA), Universidad Nacional de La Plata (UNLP), CCT La Plata-CONICET, La Plata, Argentina.

[2] CIHIDECAR-CONICET, Departamento de Química Orgánica, FCEyN, Universidad de Buenos Aires, Ciudad Universitaria, Buenos Aires, Argentina

[3] Department of Chemistry, Brooklyn College, City University of New York, Brooklyn, NY, USA

[4] Ph.D. Program in Chemistry, The Graduate Center of the City University of New York, New York, NY, USA

[5] Department of Natural Sciences, Baruch College, City University of New York, New York, NY, USA

* Corresponding author e-mail: mvignoni@inifta.unlp.edu.ar (Mariana Vignoni)

ABSTRACT

Here, we provide mechanistic insight to the photocleavage of a compound in the folate family, namely pteroic acid. A *bis*-decyl chain derivative of pteroic acid was synthesized, structurally characterized, and photochemically investigated. We showed that, like folic acid, pteroic acid and the decylated derivative undergo a photocleavage reaction in the presence of H_2O, while no reaction was observed in methanol solution. Furthermore, density functional theory calculations were carried out to predict relative stabilities of hypothetical *mono*-, *bis*-, and *tris*-decylated pteroic acid derivatives to help rationalize the regioselectivity of the *bis*-decyl pteroic acid product. Additionally, the lipophilicity of the *bis*-decyl pteroic acid appears to confer a hydrophobic property enabling an interaction with biomembranes.

INTRODUCTION

Pterins are commonly divided in two groups: (i) unconjugated pterins, bearing a methyl substituent or short hydrocarbon chain, and (ii) conjugated pterins, bearing more sizable substituents such as the *p*-aminobenzoic acid (PABA) group (1). The latter group is referred to as folates, a large family of structurally related compounds that are widespread in nature. Folates are comprised of a pteridine ring linked through a methylene bridge to a PABA unit, which, in turn, is linked to one or more L-glutamic acid residues. Folates, such as folic acid [pteroyl-L-glutamic acid (PteGlu, Figure 1)], undergo photooxidative cleavage when exposed to UVA light and oxygen, generating unconjugated pterins which themselves bear enhanced photosensitizing properties (2, 3). One important target for molecules with photosensitizing properties is the phospholipid membrane. Taking into account that pteridines possess some water-solubility, but almost no solubility in hydrophobic solvents, an advancement to the field has been the appending of decyl chains to pterin and lumazine compounds to increase lipophilicity for biomembrane localization in the hopes of selectively targeting photodynamic stress (4–7). Nonetheless, to date, the synthesis and testing of a *bis*-substituted lipophilic pteroic acid (Pte) derivative with the capacity to photooxidatively cleave is yet to be achieved, which is the aim of this work.

<Figure 1>

Lipid peroxidation may be produced in various physiological and pathological processes, involving cholesterol, glycolipids and phospholipids of biomembranes (8, 9). Several mechanisms can be implicated, being the light-mediated process one of the most important ones. Photosensitized oxidation reactions can take place through two different mechanism: *i*) a direct reaction between the triplet excited state of the photosensitizer and the target molecule, by electron transfer or hydrogen abstraction with the generation of radicals (type I mechanism), *ii*) via singlet oxygen ($^1O_2$) production by energy transfer from the triplet excited state of the photosensitizer to dissolved oxygen and the consequently reaction between $^1O_2$ and the target molecule (type II mechanism) (10, 11). The first mechanism corresponds to contact-dependent pathways where lipophilic photosensitizers interacting with lipid membranes are involved. On the other hand, type II mechanism engaging $^1O_2$ correlates with contact-independent pathways, employing lipophilic or hydrophilic photosensitizers (6, 12, 13).

Folates can differ structurally based not only on the oxidation state of the pterin ring, but also in the substituent type at the N^5 and N^{10} positions and the number of glutamic acid residues that are linked one to another via γ-glutamyl linkages (14). PteGlu is a stable vitamin of the folate family which bears good stability, but can be converted into enzymatically active forms, by reduction of the pteridine unit to dihydro- and tetrahydro-folate by the action of a dihydrofolate reductase. Tetrahydrofolate and its derivatives act as coenzymes in one-carbon transfer reactions required in the biosynthesis of pyrimidines and purines nucleotides for DNA formation and repair, and also in the amino acid metabolism (15). It has been observed that folate deficiency is related to several diseases such as neural tube defects (16, 17), megaloblastic anemia (18), cardiovascular diseases (19) and some types of cancer (20, 21). Since 1940s, the photochemistry of PteGlu has been extensively investigated as a model of folates, either in aqueous solutions or other media (2, 22–26). Under UVB/A irradiation, PteGlu photooxidatively cleavage yielding 6-formylpterin (Fop) and PABA-Glu. Later on and upon further irradiation, Fop is transformed into 6-carboxypterin (Cap).

Unconjugated aromatic pterins, like pterin (Ptr), Fop, Cap and biopterin, are modestly soluble in H_2O and capable of photosensitizing nucleotides, amino acids and proteins (27–31), and causing cell death (32). It has been shown that Ptr can photooxidize lipids that are enriched in polyunsaturated fatty acids (PUFAs), while also being capable of crossing the phospholipid membranes (33). To increase the interaction of these compounds with the lipid membrane, in the last few years we have described the conjugation of a decyl carbon chain to different pteridine derivatives, using a nucleophilic substitution (S_N2) reaction. Depending on the structure of the reactant, the decyl chain was attached in different positions of the double ring: to the O^4 or N^3 for Ptr (4) or to N^3/N^1 for lumazine (Lum) (5). In contrast for Cap, due to the presence of the carboxylic group, the carbon chain was added in that position, yielding an ester group (34). These lipophilic alkyl derivatives have been shown to localize in biomembranes leading to membrane damage upon UVA irradiation, which is of fundamental interest.

Previously, we reported on a self-sensitized photocleavage of a 3-component conjugate [chlorin sensitizer, *S,S*-chiral cyclohexane and ethene building blocks] that upon exposure of the ethene site to $^1O_2$ released the sensitizer portion (35). We had also focused on topics of compound conjugation and solubility tuning through PEGylation (*mono*, *bis*, and *tris*) (36) and long chain alkylation (37), with further interests in natural compounds bearing double-segments of long alkyl chains, such as the cytotoxin asimicin.

Taking into account the chemical structure of Pte and PteGlu (Figure 1), we assumed the photocleavage process of the former would be similar to what is observed for PteGlu, yielding Fop and PABA as photoproducts. Therefore, we hypothesized that alkylation of Pte would lead to a lipophilic compound able to interact with lipid membranes, and to undergo photodegradation generating unconjugated pterin photosensitizers, such as Fop and Cap. Moreover, we sought insight to whether Pte would be *mono*- or *bis*-decylated and whether the alkylation occurs at *O*- vs *N*-positions of Pte.

In this work, a lipophilic pterin derivative, namely decyl 4-(((2-amino-4-decyloxypteridin-6-yl)methyl)amino)benzoic acid (abbreviated hereafter as *bis*-decyl-

Pte) has been synthesized, and bears two alkyl chains, one of them linked to the O^4 position of the pterin moiety and the other one, linked to PABA carboxylic acid group. We also computed regiochemical patterns arising from the nucleophilic substitution (S_N2) reactions with the compound. DFT results have provided insight into the alkylation patterns and observed regioselectivity in the synthesis of *bis*-decyl-Pte. We also report on spectroscopic properties and photocleavage of *bis*-decyl-Pte and compare them to Pte behavior which, to the best of our knowledge, has not been reported before. Finally, we analyze the interaction of *bis*-decyl-Pte with lipid membranes and discussed its potential use as biomembrane photosensitizer, in which ramifications are found of potential interest for membrane science and biomedical applications.

EXPERIMENTAL PART

Chemicals. Pteroic Acid (Pte, purity > 99%) was acquired from Schircks Laboratories (Switzerland). 1-Iododecane was obtained from Sigma and potassium carbonate (K_2CO_3) was obtained from Biopack. *Tris*-(hydroxymethyl)aminomethane (Tris) was acquired from Genbiotech. 1,2-Dioleoyl-*sn*-glycero-3-phosphocholine (DOPC, powder, ≥ 99%,) was purchased from Avanti Polar Lipids Inc. Dichloromethane (DCM), *N,N*-dimethylacetamide (DMA) and chloroform-*d* were from Cicarelli. HPLC grade acetonitrile (ACN) and methanol (MeOH) were from PanReac AppliChem. H_2O was purified using a deionization system.

Synthesis. Pte (5 mg, 0.016 mmol) was dissolved in DMA (6 mL) and potassium carbonate was added (2.2 mg, 0.016 mmol). After sonication the mixture was sparged with nitrogen for 20 min and 1-iododecane (6.9 µL, 0.032 mmol) was added. The reaction mixture was positioned into an oil bath at 70 °C for 5 h. After evaporation of the solvent under vacuum, a solid residue was obtained and treated first with NaCl (s.s.) (10 mL) and then was extracted with DCM (3 × 50 mL). Afterwards, the organic phase was dried over Na_2SO_4, filtered, and evaporated, obtaining a light-yellow solid residue. This sample was worked up by silica gel column chromatography (eluent: DCM 100% followed by DCM−MeOH mixtures) and the final product was obtained unpurified. To finish the purification, a preparative HPLC was used.

Bis-decyl-Pte. Yield: 1.08 mg (22 %), purity 98 %. Rf (MeOH/DCM 5:95 v/v): 0.37. ^{1}H NMR (500 MHz, $CDCl_3$): δ 8.83 (s, 1H, H-4), 7.89 (d, *J* = 8.8 Hz, 2H, H-10), 6.68 (d, *J* = 8.8 Hz, 2H, H-9), 5.33 (sa, 2H, NH_2), 5.21 (t, *J* = 5.4 Hz, 1H, NH), 4.66 (d, *J* = 5.3 Hz, 2H, H-7), 4.59 (t, J = 7.0 Hz, 2H, Hα'), 4.25 (t, *J* = 6.7 Hz, 2H, H-α), 1.95 (q, *J* = 7.7 Hz, 2H, Hβ'), 1.73 (q, *J* = 6.7 Hz, 2H, H-β), 0.88 (t, *J* = 7.06 Hz, 6H, Hω and Hω'). ^{13}CNMR (126 MHz, $CDCl_3$): δ 167.67 (C-4), 166.91 (C-7'), 156.75 (C-6'), 151.02 (C-4'), 150.23 (C-5'), 148.54 (C-6), 131.73 (C-2'), 123.08 (C-4a), 120.02 (C-1'), 112.16 (C-3'), 68.76 (C-α'), 64.68 (C-α), 46.86 (C-9), 29.00 (C-β'), 28.62 (C-β), 22.84 ($C_{ω-1}$ and $C_{ω-1'}$), 14.27 (Cω and Cω'). HRMS (ESI): *m/z* calcd for $C_{34}H_{53}N_6O_3$ [$M+H^+$] = 593.4173, found 593.4188.

Absorption measurements. Absorption spectra were recorded on a Shimadzu UV-1800 spectrophotometer, using quartz cells of 0.4 or 1 cm optical path length.

Nuclear magnetic resonance spectroscopy. Spectra were recorded on a Bruker Avance Neo 500 (500 MHz for ^{1}H and 125.1 MHz for ^{13}C). Chemical shifts (δ) are given in ppm downfield from TMS as the internal standard. Coupling constant (*J*) values are in Hz.

High-performance liquid chromatography (HPLC). A Prominence Shimadzu equipment was used (communications bus module CBM-20, on-line degasser DGU-20A5, solvent delivery module LC-20AT, auto sampler SIL-20A HT, column oven CTO-

10AS VP and photodiode array (PDA) detector SPD-M20A), with a Synergi Polar-RP analytical column (ether-linked phenyl phase with polar endcapping, 150 x 4.6 mm, 4 µm, Phenomenex) for separation. Different conditions were set depending on the experiment: a) flow rate of 0.3 mL min^{-1} and 100% MeOH as mobile phase, b) flow rate of 0.6 mL min^{-1} and 80 % ACN and 20 % Ammonium Acetate ($AcNH_4$, 10 mM), c) flow rate of 0.6 mL min^{-1} and the mobile phase consisted of ACN (solvent A) and formic acid (FA, 10 mM, pH 4) (solvent B). The gradient elution started with 96 % solvent B for 10 min, from 10 to 14 min solvent B decreased from 96 to 82 %, stayed at 82 % up to 24 min, then increased from 24 to 28 min to 96 % and maintain for 7 min. The total run time was 35 min.

Preparative high-performance liquid chromatography (P-HPLC). A preparative Shimadzu Prominence equipment was employed (communications bus module CBM-20, solvent delivery module LC-20AT, UV/vis detector SPD-20A, fraction collector FRC-10A and manual injector). A Synergi Polar-RP 80 Å semi-prep column (4µm, 250 x 10 mm, Phenomenex) was used for separation with 100% MeOH as mobile phase and a flow rate of 1.5 mL min^{-1}.

Molecular exclusion chromatography. Sephadex G-50 was equilibrated in pure H_2O and poured into a 0.8 × 22 cm column. Then, the column was equilibrated with Tris 20 mM buffer pH 8. Samples were eluted with the same buffer and collected in 1 ml fractions

High Resolution Mass spectrometry analysis. Molecular weight values were determined using direct injection ESI-MS and UPL-MS techniques. *i)* Direct injection high resolution electrospray ionization mass spectrometry analysis (DI-MS) was performed in positive ion mode using the mass spectrometer BRUKER microTOF-Q II equipped with CID (cell induce decomposition). Acquisition parameters: capillary temperature, 180 °C; nebulizer pressure, 0.4 Bar; capillary voltage, 4000 V; dry heater temperature, 200 °C; end plate offset voltage, −500 V; set dry gas at 4.0 l min^{-1}; in MS/MS experiments CID RF, 150.0 Vpp. Samples were dissolved in MeOH or ACN/$AcNH_4$ (80/20). *ii)* Xevo QTof-MS (Waters) spectrometer coupled with a UPLC (Waters) (UPLC-MS) was used, with a Zorbax Eclipse Plus C18 column (4.6 x 100 mm, 3.5 µm, Agilent). The mobile phase was 5% of formic acid solution 0.1% and 95% of 0.1% formic acid in acetonitrile, at a flow rate of 0.3 mL min^{-1}. The injection volume was of 10 µL. The ESI source was operated in positive ionization mode with the capillary voltage at 3.5 kV; temperature of the source and desolvation was 120 and 400 °C, respectively; cone and desolvation gas flows were 10 and 800 L h^{-1}, respectively. Leucine-enkephalin was used as the lock mass generating an [M + H]+ ion (m/z 556.2771) at a concentration of 250 pg/mL and flow rate of 50 µL min^{-1} to ensure accuracy during the MS analysis.

Steady-state irradiation. The continuous photolysis of compounds in air-equilibrated solutions was carried out irradiating in quartz cells (0.5 cm optical path length). One UVA lamp with emission centered at 365 nm [band width (fwhm) 20 nm] was employed as radiation source. To measure the incident photon flux density ($q^{0,V}_{n,p}$), Aberchrome 540 (Aberchromics Ltd.) was used as an actinometer (38). The acquired value was 5.6 (± 0.2) $\times 10^{-5}$ $EL^{-1}s^{-1}$. Values of the photon flux absorbed ($q^{a,V}_{n,p}$),were calculated from ($q^{0,V}_{n,p}$), according to the Lambert–Beer law:

$$q^{a,V}_{n,p} = q^{0,V}_{n,p} (1 - 10^{-A})$$

where A is the absorbance of the reactant at the excitation wavelength.

Quantum yield determinations. The quantum yields of reactant disappearance (Φ_R) were determined and values were obtained using the following equations:

$\Phi_R = -(d[R]/dt)_0 / q^{a,V}_{n,p}$

where $(d[R]/dt)_0$ is the initial rate of reactant consumption and $q^{a,V}_{n,p}$ is the photon flux absorbed by the reactant. The initial rates were obtained from the slope of the corresponding plots of concentration vs. irradiation time within such time windows. The evolution of the concentrations during irradiation was followed by HPLC (vide supra).

Hydrogen peroxide (H_2O_2) measurements. The quantification of H_2O_2 was carried out with a Cholesterol Kit (Wiener Laboratorios S.A.I.C.), in which H_2O_2 reacted with 4-aminophenazone and phenol (39, 40). Briefly, post-irradiated samples of *bis*-decyl-Pte were combined with the Cholesterol Kit reagents. The absorbance at 505 nm of the resulting mixture was measured after 30 min of incubation at room temperature, using the reagent as a blank. Aqueous H_2O_2 solutions prepared from commercial standards were employed for calibration.

Computational methods. The theoretical calculations were conducted with the Gaussian16 program (revision C.01) (41). B3LYP was used along with the Dunning basis set, D95(d,p), which performed well based on previous reports of alkyl-chain conjugated pterins and lumazines (5, 42). Enthalpy values were thermal corrected at 298.15 K and 1 atm.

RESULTS

The results are presented in the following subsections: (1) synthesis and characterization of the decylated pteroic acid; (2) DFT calculated results of the *bis*-decyl-Pte, as well as hypothetical *mono*-, *bis*- and *tris*-decylated Pte derivatives; (3) spectral features of *bis*-decyl-Pte; (4) photocleaving behavior and membrane interaction of Pte and *bis*-decyl-Pte.

Synthesis of alkylated pteroic acid derivative

A bimolecular nucleophilic substitution (S_N2) reaction was carried out for the alkylation reaction of Pte according to the methodology previously reported for alkylation of Ptr, Cap and Lum (4, 5, 34). Thus, the alkylation reaction was performed dissolving Pte in DMA in the presence of solid K_2CO_3 and 1-iododecane and the reaction was heated at 70 ºC for 5 hr. A main product (*bis*-decyl-Pte; see Scheme 1) was obtained in 22 % yield after chromatographic purification showing purity higher than 98 % according to HPLC control. Furthermore, *bis*-decyl-Pte showed a noticeable high solubility in organic solvents when was compared to native Pte, as it was observed for cases of alkylated pterin and lumazine derivatives (4, 5).

<Scheme 1>

The elucidation of the chemical structure and fully characterization of compound *bis*-decyl-Pte was carried out by using 1D and 2D NMR spectroscopy (see NMR spectra in SI). Furthermore, to verify the position of the two decyl chains, HMBC experiment was performed and the partial contour plot is depicted in Figure 2. The cross-peaks shown in the figure clearly demonstrate the satisfactorily correlations between both the α and α' methylene groups $C^{7'}$ and C^4, respectively. Indeed, the signal belonging to methylene α' protons located at 4.59 ppm correlates with the signal of C^4 at 165.7 ppm leading to conclude that the decyl chain reacted with the phenol group of pterin (see orange arrow in Figure 2). Likewise, the proton signal of methylene α located at 4.25 ppm correlates with the carbonyl group ($C^{7'}$) whose chemical shift is centered at 166.7 ppm (see blue arrow in Figure 2) demonstrating that the decyl chain is bonded to the carboxylic group of the PABA residue.

<Figure 2>

To confirm the chemical structure of *bis*-decyl-Pte, high resolution mass spectrometry analysis (DI-MS) was carried out. The spectra showed a main signal at *m/z* 593.4188, which corresponds to the protonated molecular ion $[M+H^+]$ of a compound M having the Pte moiety with two additional decyl chains attached ($M = C_{34}H_{52}N_6O_3$) (Figure S6, SI). Also, tandem mass spectrometry (MS/MS experiments, CID mode) selecting $[M+H]^+$ as precursor ion showed several diagnostic fragments; firstly, even though small, those corresponding to the loss of a decyl-chain $C_{10}H_{20}$ $[(M+H)^+-C_{10}H_{20}]$ with a peak at *m/z* 453.2589 and the loss of a decyl-chain and H_2O $[(M+H)^+-C_{10}H_{20}-H_2O]$ with a peak at *m/z* 435.2502. The former can be formed by McLafferty-like rearrangements involving the ester moiety (–COO-$C_{10}H_{21}$) and/or the pterin moiety (–N=C–O-$C_{10}H_{21}$) and the latter is the characteristic loss of H_2O by the –COOH group, yielded after the McLafferty reaction on the ester moiety (–COO-$C_{10}H_{21}$ $\rightarrow$ –COOH + $C_{10}H_{20}$). This suggests that one of the decyl chains is attached to the carboxylic group of the PABA part of the moiety as an ester group. The two most important fragments observed correspond to the loss of two decyl-chains ($[M+H]^+-C_{20}H_{40}$) and two decyl-chains + H_2O ($[M+H]^+-C_{20}H_{40}-H_2O$) with peaks at *m/z* 313.1045 and 295.0933, respectively. The former indicates that both McLafferty rearrangements took place successively from the precursor ion $[M+H]^+$ and the latter agrees with the loss of H_2O afterwards. The peak at *m/z* 176.0567 corresponding to the pterin moiety itself was also observed (Figure S7, SI).

Therefore, the above experimental data from NMR and DI-MS studies conclude that one of the decyl-chain is attached to the carboxylic acid group of de PABA moiety of the molecule, as it was observed with CapC (34), and the other decyl-chain is attached to the O^4 of the pterin moiety. To help deduce the formation of the experimentally detected *bis*-decyl-Pte, DFT computations were carried out to predict relative energies of various regio-connections of the decyl group to Pte.

DFT Calculations

Gas-phase DFT computations were used to predict relative energies and analyze hypothetical *mono*-, *bis*-, and *tris*-decylated analogs to help rationalize the experimental formation of *bis*-decyl-Pte (also called ***bis*-2A** in Figure 4). Figures 3-5 show the relative free energies (ΔG). The *mono*-decylated combinations in Figure 3 show that the O^4 ***mono*-1A** is 5.4 kcal/mol and $O^{7'}$ ***mono*-1B** 3.0 kcal/mol less stable than the N^2 ***mono*-1D**. Thus, whether experimentally observed ***bis*-2A** precedes initially by ***mono*-1A** or ***mono*-1B** point to kinetic rather than thermodynamic control in the decylation process. The *bis*-decylated combinations in Figure 4 show that the O^4,$O^{7'}$ ***bis*-2A** is 6.5 kcal/mol less stable and N^2,O^4 ***bis*-2B** 3.5 kcal/mol or N^2,N^2 ***bis*-2B** 2.1 kcal/mol less stable than N^2,N^3 ***bis*-2F**. Interestingly, the experimentally observed ***bis*-2A** is clearly the least energetically stable *bis*-decylated compound of the series, offering kinetic control as an explanation of the origin of the regioselectivity. The *tris*-decylated combinations in Figure 5 show that steric incumbrance leads to the high energy of the N^2, N^2, N^3 ***tris*-3A** of 9.3 kcal/mol and N^2,N^2,O^4 ***tris*-3B** 5.4 kcal/mol which are less stable relative to N^2,N^3,$O^{7'}$ ***tris*-3E**. If a *tris*-Pte were to experimentally form, or at least form in minor amounts, the DFT results lead us to suggest that N^2,O^4,$O^{7'}$ ***tris*-3C** would be the most likely structure. Interestingly, in our previous work, in *N,N*-dimethylformamide (DMF) solvent DMF condensation at the N^2 site was readily observed (4, 34), although in the current work we used DMA solvent, where no condensation at N^2 site arose.

<Figure 3>

<Figure 4>

<Figure 5>

Spectroscopic properties

Pte presents several acid-basic equilibria with three detected pK_a values: 2.29 ± 0.03, 4.72 ± 0.01 and 7.98 ± 0.03, for N^1, carboxylic group and $N^3H–C^4O$ lactam group, respectively (43). The pK_a of the lactam group is the most important one since it is close to the physiological pH. Therefore, the absorption molar coefficient for both acid (monoanionic) and basic (dianionic) forms of Pte in aqueous solution was obtained (Figure 6.a). The features of the absorption spectrum of Pte and its dependence on the pH can be interpreted taking into account previous studies (44). The pterin chromophore typically exhibits two main absorption bands. The high-energy band of the acid form is less intense and red-shifted in comparison with the corresponding band of the basic form; on the other hand, the low-energy band of the acid forms is less intense, but blue-shifted in comparison with the corresponding band of the basic form. Conjugated pterins show, in addition to the two absorption bands of the pterin chromophores, a band corresponding to the PABA unit, which does not undergo ionization and therefore its spectrum does not significantly change with the pH. While the basic form of Pte shows the three absorption bands described, for its acid form the high-energy band of pterin and the PABA band are superimposed, which results in a spectrum of two bands. This behavior can also be observed for folic acid (44). Figure 6.b shows the absorption spectrum of *bis*-decyl-Pte in MeOH, with three absorption bands. The highest energy band is centered at 229 nm, similar to the one observed for *O*-decyl-Ptr; a second band at 298 nm which corresponds to the PABA unit; and the UVA band centered at 367 nm, similar to the one detected for the basic form of Pte, which is in agreement with the fact that the decyl chain is attached to the O^4 of the pterin moiety.

Emission of *bis*-decyl-Pte was studied in H_2O and MeOH, and in both media the fluorescence intensity was negligible. This is in accordance with the behavior observed for PteGlu and Pte, where the large substituent at position 6 on the pterin moiety acts as an “internal quencher” enhancing the radiationless deactivation of the singlet excited state and, consequently, drastically reducing the fluorescence quantum yield (44, 45). The mechanism of the internal deactivation has been proposed to be an electron transfer from the PABA ring to the pterin moiety, which is consistent with the result that no emission was observed in either solvent.

<Figure 6>

Photodegradation and membrane interaction

In spite of the biological importance of Pte and its similarity to PteGlu, Pte’s photochemical stability has not been previously reported. PteGlu is known to be unstable to UVA radiation and fragment to Fop and PABA-Glu (2). Thus, we investigated the photodegradation of Pte in aqueous solution at pH 6.7 with irradiation at different time intervals and the absorption spectra recorded. Concentration of Pte was kept below 30 μM, since the solubility in H_2O at this pH is ~ 0.019 mg/mL (60 μM). Although changes in absorption were small (Figure S9), HPLC analyses revealed the consumption of Pte and formation of PABA, Fop, Cap and Ptr (Figure 7). As previously observed for PteGlu, Pte undergoes an excision of the methylene bridge with the incorporation of a H_2O molecule, thereby generating PABA and Fop. Since Fop is photolabile, the formation of Cap is also observed (24), which later generates Ptr by decarboxylation (46). The proposed photocleavage mechanism is shown in Scheme 2. Moreover, and as observed for PteGlu (25), H_2O_2 was detected during this photochemical reaction, which points to an electron transfer process (47).

<Figure 7>

<Scheme 2>

Due to the low solubility of *bis*-decyl-Pte in H_2O (~ 0.0059 mg/mL) compared to Pte (~ 0.019 mg/mL), we elected to study the photodegradation of *bis*-decyl-Pte in MeOH, as well as in MeOH/H_2O (50/50). After 60 min of UVA irradiation, no significant changes in the in the concentration of *bis*-decyl-Pte in MeOH were observed (Figure 8). However, when H_2O was present in the MeOH, a noticeable consumption of *bis*-decyl-Pte was detected. This result is similar to that observed for Pte, in which H_2O facilitates in the photodegradation process, likely being due to mechanistic similarities to the Pte photodegradation itself. Both quantum yields of consumption were calculated, obtaining a value of $(7 \pm 2) \times 10^{-4}$ for Pte in aqueous solution and $(8 \pm 1) \times 10^{-4}$ for *bis*-decyl-Pte in MeOH/H_2O (50/50).

<Figure 8>

Next, we analyzed the photoproducts arising from *bis*-decyl-Pte using HPLC. Five well-defined peaks arose and their areas increased upon the irradiation of *bis*-decyl-Pte (Figure 9). Analysis of the absorption spectra of products P1, P2, P4 and P5 suggests that are pteridine derivatives, while P3 which has no absorption in the UVA region is not. P1, P2 and P3 were characterized by mass spectrometry (UPLC-MS). P1 showed an *m/z* value of 348.2010 corresponding to the $[M+H^+]$ of a compound M = decyl-Cap (M = $C_{17}H_{25}N_5O_3$) and a calculated $[M+H^+]$ value of 348.2036 (Figure S10). Regarding P2, an *m/z* value of 332.2060 was observed, which corresponds to the $[M+H^+]$ of a compound M = decyl-Fop (M = $C_{17}H_{25}N_5O_2$) and a calculated $[M+H^+]$ value of 332.2087 (Figure S11). Moreover, and as expected considering the absorption spectra, P3 showed an *m/z* value of 278.2140 corresponding to the $[M+H^+]$ of a compound M = decyl-PABA (M = $C_{17}H_{27}NO_2$) and a calculated $[M+H^+]$ value of 278.2120 (Figure S12). This shows that *bis*-decyl-Pte undergoes a photocleavage at the methylene bridge similar to that seen in the native Pte, and that a hydrolytic step with H_2O is needed in the reaction since *bis*-decyl-Pte is photostable in MeOH solution (Figure 8). Nevertheless, there must be another degradation mechanism since two other compounds (P4 and P5) are formed during the irradiation. As no *m/z* value was obtained in these conditions for P4 and P5, we proposed a partial degradation mechanism showing only the photocleavage of *bis*-decyl-Pte (Scheme 2).

<Figure 9>

Taking into account that *bis*-decyl-Pte has no detectable fluorescence emission, we were unable to quantify the interaction of the photosensitizer with the lipid membrane through a binding constant determination, as completed before for other alkylated pterin derivatives (4, 5, 34). Nevertheless, qualitative evidence was collected for the interaction of *bis*-decyl-Pte with lipid membrane using size exclusion chromatography. DOPC LUVs containing ~ 2 % of the compound were passed through the column and fractions were collected and analyzed by spectrophotometry, to detect the light scattering of LUVs. In addition, fractions were diluted in MeOH to disaggregate the vesicles and injected in the HPLC equipment to detect the compound. As shown in Figure 10, the elution of LUVs and *bis*-decyl-Pte are detected in the same fractions (mainly 3 and 4) indicating that the compound interacts with the lipid membrane. The same experiments were performed with native Pte and the compound was detected mainly between the fractions 10 to 15, indicating that it does not interact with lipid membranes (Figure S11).

These findings make *bis*-decyl-Pte an interesting compound to use as a lipophilic photosensitizer, since is not only able to interact with biomembranes but could also generate additional compounds which may act as photosensitizers their self.

<Figure 10>

DISCUSSION

As mentioned in the Introduction, our previous studies demonstrated that decylation gives the pterin moiety the capacity to intercalate in lipid membrane, while retaining its photosensitizing properties (4, 5). Therefore, conjugation of an alkyl chain could serve as a simple and effective tool to convert an otherwise hydrophilic photosensitizer into a lipophilic photosensitizer, to potentially induce photodamage in lipid bilayers. Taking into account the importance of folate-related compounds to living organisms, their photochemical properties and our previous work on decylation of pterins (4, 5, 34), arises the idea of exploring lipophilic derivatives of folate-related compounds.

Therefore, we have synthesized a new *bis*-decyl-Pte from pteroic acid (Pte), through a nucleophilic substitution reaction (S_N2). *O*-Alkylation of Pte is observed both at the keto position O^4, which is similar to the main products generated in our previous report on alkyl pterin derivatives (4); and at the carboxylic acid position of the PABAgroup, similar to what we observed in our previous report on a carboxypterin derivative (34). DFT results point to the formation of *bis*-decyl-Pte as kinetic rather than thermodynamic control in the decylation process, as it was detected in the case of pterin (42). When compared to native Pte, the *bis*-decyl-Pte has similar absorption spectra to the basic form of Pte, in agreement with the alkylation in the keto position O^4. Our results show that solubility in H_2O is about 3-fold lower for *bis*-decyl-Pte (~ 0.0059 mg/mL) compared to Pte (~ 0.019 mg/mL). Interestingly, no detectable photooxidation of *bis*-decyl-Pte is observed during UVA irradiation in MeOH solvent, but in the presence of water in H_2O/MeOH degradation is readily observed. Thus, in the latter solvent, *bis*-decyl-Pte suffers from a photooxidation cleavage in the same methylene bridge as native Pte and also PteGlu (24). This is in accordant with hydrolysis as a key component in the cleavage reaction, consistent with the evidence of alkyl-Fop, alkyl-Cap and alkyl-PABA detected by mass spectrometry as photoproducts. In addition, as *bis*-decyl-Pte is able to interact with lipid membranes, further efforts are focused on detecting if this photocleavage is also observed when *bis*-decyl-Pte is interacting with the biomembranes and if these photoproducts remained inside the lipid membrane or are released to the bulk water.

On the other hand, folate cellular uptake is mediated by the folate-binding proteins, referred to as folate receptors (FR), in which folate binding can triggers endocytosis (48, 49). Intriguingly, while its expression is negligible in healthy cells, a number of human cancer cell lines bear over-expressed levels of FR (50, 51). Therefore, and to avoid damage to healthy cells and tissues, there is an increasing use of the folate groups to selectively deliver therapeutic and diagnostic agents (52–54). Since FR binds directly to the pteroyl moiety while glutamate stays out of the receptors binding pocket (55), great efforts are focused on the development of pteroic acid derivatives.

In our case, *bis*-decyl-Pte may have a possibly dual target approach: the affinity to lipid membranes and the binding to FR. Moreover, *bis*-decyl-Pte would potentially release upon irradiation different lipophilic unconjugated pterin with photosensitizing properties. Therefore, *bis*-decyl-Pte may have a strong photosensitizer activity producing not only lipid peroxidation in membranes but also entering to the cell to generate important cell damage and death. Triggered by the findings presented in this work, several studies arise as needed to expand the information aimed to the development of a new generation of photosensitizers with selectivity towards tumor cells due to the capability to bind specific receptors over expressed in the target cells. In this regard, the following properties of *bis*-decyl-Pte will be addressed in the near future: i) cellular uptake mechanism, ii) the efficiency to photoinduce cell death, iii) the efficiency to photoinduce lipid peroxidation and membrane structural damage and iv) the photochemistry when associated to membranes. Finally, the synthesis and analysis of new lipohilic photosensitizers derived from Pte will also be addressed.

CONCLUSIONS

A new lipophilic folate derivative was synthesized [4-(((2-amino-4-decyloxypteridin-6-yl)methyl)amino)benzoic acid (*bis*-decyl-Pte)]. *Bis*-decyl-Pte was not only structurally characterized, but also photophysically characterized. Decylation of Pte was found to arise at keto O^4 and at the PABA carboxylic acid group, pointing to a kinetically-controlled process based on results from DFT calculations. The photochemistry of Pte and *bis*-decyl-Pte was investigated in various solvents, in which the photocleavage is attributed to involve hydrolysis of the methylene bridge. Moreover, *bis*-decyl-Pte is able to interact with lipid membranes. Future efforts will be focused on investigating the photosensitizing properties of this compound over lipid membranes, and also the cellular uptake and photodamage.

ACKNOWLEDGMENTS

This work was partially supported by Agencia Nacional de Promoción Científica y Tecnológica (ANPCyT-Grants PICT 2016-1189, 2016-0130, 2017-0925 and 2019-3416), Universidad Nacional de La Plata (UNLP-Grant X840) and Consejo Nacional de Investigaciones Científicas y Técnicas (CONICET, PUE 2017-22920170100100CO). MV, AHT and AG thank CONICET and NSF for supporting their collaboration through a Bilateral Cooperation Programme Level I. EMG acknowledges support from the National Science Foundation (NSF) (CHE-1956098) and PSC-CUNY (63367-00 51-A). AG also acknowledges support from the NSF (CHE-2154133). We deeply acknowledge Drs. María Noel Urrutia and Patricia L. Schilardi for their assistance and for the access to facilities for the synthetic experiments. Carmen Clemente Martínez (Instituto de Tecnología Química, Universidad Politécnica de Valencia) is acknowledged for her technical help during the UPLC-HRMS experiments. JLF thanks ANPCyT, and MJS and MIQ thank CONICET for doctoral research fellowships, GP, REB, SB, AHT and MV are research members of CONICET. This work used Comet and Expanse, the Extreme Science and Engineering Discovery Environment (XSEDE) clusters at the San Diego Supercomputer Center, which are supported by the NSF (ACI-1548562) through allocations TG-CHE180060 (EMG) and CHE200050 (AG).

ORCID

Sergio M. Bonesi: 0000-0003-0722-339X

Rosa Erra-Balsells: 0000-0003-0169-0173

José Luis Fonseca: 0000-0002-6188-3498

Edyta M. Greer: 0000-0003-4283-0523

Alexander Greer: 0000-0003-4444-9099

Gabriela Petroselli: 0000-0002-8602-3611

Andrés H. Thomas: 0000-0002-8054-7799

Mariana Vignoni: 0000-0003-4506-7527

SUPPORTING INFORMATION

Additional supporting information may be found online in the Supporting Information section at the end of the article:

Figure S1. 500 MHz ^{1}H-NMR spectrum of *bis*-decyl-Pte in $CDCl_3$.

Figure S2. 127.5 MHz ^{13}C-NMR spectrum of *bis*-decyl-Pte in $CDCl_3$.

Figure S3. 500 MHz DFQ-COSY spectrum of *bis*-decyl-Pte in $CDCl_3$.

Figure S4. 500 MHz HSQC-DEPT spectrum of *bis*-decyl-Pte in $CDCl_3$.

Figure S5. 500 MHz HMBC spectrum of *bis*-decyl-Pte in $CDCl_3$.

Figure S6. DI-MS spectrum of *bis*-decyl-Pte.

Figure S7. DI-MS/MS spectrum of *bis*-decyl-Pte.

Figure S8. B3LYP/D95(d,p) calculated structures and energies of *mono*-decylated pteroic acids (***mono*-1A**, ***mono*-1B**, ***mono*-1C**, and ***mono*-1D**), *bis*-decylated pteroic acids (***bis*-2A**, ***bis*-2B**, ***bis*-2C**, ***bis*-2D**, ***bis*-2E**, and ***bis*-2F**), and *tris*-decylated pteroic acids (***tris*-3A**, ***tris*-3B**, ***tris*-3C**, ***tris*-3D**, and ***tris*-3E**) are reported.

Figure S9. Time evolution of the absorption spectra of Pte in air-equilibrated aqueous solutions under UVA irradiation.

Figure S10. UPLC-MS spectrum of P1.

Figure S11. UPLC-MS spectrum of P2.

Figure S12. UPLC-MS spectrum of P3.

Figure S13**.** Elution profiles of size exclusion chromatography performed on DOPC LUVs with Pte.

REFERENCES

1. Lorente, C. and Thomas, A. H. (2006) Photophysics and photochemistry of pterins in aqueous solution. *Acc. Chem. Res.* **39**, 395–402.

2. Dántola, M. L., Urrutia, M. N. and Thomas, A. H. (2018) Effect of pterin impurities on the fluorescence and photochemistry of commercial folic acid. *J. Photochem. Photobiol. B Biol.* **181**, 157–163. https://doi.org/https://doi.org/10.1016/j.jphotobiol.2018.03.007.

3. Tsyupka, D. V., Mordovina, E. A., Sindeeva, O. A., Sapelkin, A. V., Sukhorukov, G. B. and Goryacheva, I. Y. (2021) High-fluorescent product of folic acid photodegradation: Optical properties and cell effect. *J. Photochem. Photobiol. A Chem.* **407**, 113045. https://doi.org/10.1016/j.jphotochem.2020.113045.

4. Vignoni, M., Walalawela, N., Bonesi, S. M., Greer, A. and Thomas, A. H. (2018) Lipophilic decyl chain-pterin conjugates with sensitizer properties. *Mol. Pharm.* **15**, 798–807. https://doi.org/10.1021/acs.molpharmaceut.7b00136.

5. Sosa, M. J., Urrutia, M. N., Schilardi, P. L., Quindt, M. I., Bonesi, S. M., Denburg, D., Vignoni, M., Greer, A., Greer, E. M. and Thomas, A. H. (2021) Mono- and bis-alkylated lumazine sensitizers: Synthetic, molecular orbital theory, nucleophilic index and photochemical studies. *Photochem. Photobiol.* **97**, 80–90. https://doi.org/10.1111/php.13310.

6. Vignoni, A., Layana, C., Junqueira, H. C., Thomas, A. H., Itri, R., Baptista, M. S. and Vignoni, M. (2021) Alkylation of a hydrophilic photosensitizer enhances the contact-dependent photo-induced oxidation of phospholipid membranes. *Dye. Pigment.* **187**, 109131. https://doi.org/https://doi.org/10.1016/j.dyepig.2020.109131.

7. Vignoni, M., Urrutia, M. N., Junqueira, H. C., Greer, A., Reis, A., Baptista, M. S., Itri, R. and Thomas, A. H. (2018) Photo-oxidation of unilamellar vesicles by a lipophilic pterin: deciphering biomembrane photodamage. *Langmuir* **34**, 15578–15586.

https://doi.org/10.1021/acs.langmuir.8b03302.

8. Girotti, A. W. (2001) Photosensitized oxidation of membrane lipids: Reaction pathways, cytotoxic effects, and cytoprotective mechanisms. *J. Photochem. Photobiol. B Biol.* **63**, 103–113.

9. Girotti, A. W. and Korytowski, W. (2016) Cholesterol as a natural probe for free radical-mediated lipid peroxidation in biological membranes and lipoproteins. *J. Chromatogr. B* **1019**, 202–209. https://doi.org/https://doi.org/10.1016/j.jchromb.2015.12.034.

10. Baptista, M. S., Cadet, J., Di Mascio, P., Ghogare, A. A., Greer, A., Hamblin, M. R., Lorente, C., Nunez, S. C., Ribeiro, M. S., Thomas, A. H., Vignoni, M. and Yoshimura, T. M. (2017) Type I and II photosensitized oxidation reactions: Guidelines and mechanistic pathways. *Photochem. Photobiol.* **93**, 912–919. https://doi.org/10.1111/php.12716.

11. Baptista, M. S., Cadet, J., Greer, A. and Thomas, A. H. (2021) Photosensitization reactions of biomolecules: Definition, targets and mechanisms. *Photochem. Photobiol.* **n/a**. https://doi.org/https://doi.org/10.1111/php.13470.

12. Kawai, C., Araújo-Chaves, J. C., Magrini, T., Sanches, C. O. C. C., Pinto, S. M. S., Martinho, H., Daghastanli, N. and Nantes, I. L. (2014) Photodamage in a mitochondrial membrane model modulated by the topology of cationic and anionic meso-tetrakis porphyrin free bases. *Photochem. Photobiol.* **90**, 596–608. https://doi.org/10.1111/php.12228.

13. Bacellar, I. O. L. and Baptista, M. S. (2019) Mechanisms of photosensitized lipid oxidation and membrane permeabilization. *ACS Omega* **4**, 21636–21646. https://doi.org/10.1021/acsomega.9b03244.

14. Lucock, M. (2000) Folic acid: Nutritional biochemistry, molecular biology, and role

in disease processes. *Mol. Genet. Metab.* **71**, 121–138.
15. Appling, D. R. (1991) Compartmentation of folate-mediated one-carbon metabolism in eukaryotes. *FASEB J.* **5**, 2645–2651. https://doi.org/10.1096/fasebj.5.12.1916088.
16. Prevention of neural tube defects: results of the Medical Research Council Vitamin Study. MRC Vitamin Study Research Group (1991) *Lancet* **338**, 131–137.
17. Morris, J. K., Addor, M.-C., Ballardini, E., Barisic, I., Barrachina-Bonet, L., Braz, P., Cavero-Carbonell, C., Den Hond, E., Garne, E., Gatt, M., Haeusler, M., Khoshnood, B., Lelong, N., Kinsner-Ovaskainen, A., Kiuru-Kuhlefelt, S., Klungsoyr, K., Latos-Bielenska, A., Limb, E., O'Mahony, M. T., Perthus, I., Pierini, A., Rankin, J., Rissmann, A., Rouget, F., Sayers, G., Sipek, A., Stevens, S., Tucker, D., Verellen-Dumoulin, C., de Walle, H. E. K., Wellesley, D., Wertelecki, W. and Bermejo-Sanchez, E. (2021) Prevention of neural tube defects in Europe: A public health failure. *Front. Pediatr.* **9**, A647038.
18. Aslinia, F., Mazza, J. J. and Yale, S. H. (2006) Megaloblastic anemia and other causes of macrocytosis outpatient practice tips management. *Clin. Med. Res.* **4**, 236–241.
19. Albert, C. M., Cook, N. R., Gaziano, J. M., Zaharris, E., MacFadyen, J., Danielson, E., Buring, J. E. and Manson, J. E. (2008) Effect of folic acid and B vitamins on risk of cardiovascular events and total mortality among women at high risk for cardiovascular disease: A randomized trial. *JAMA* **299**, 2027–2036. https://doi.org/10.1001/jama.299.17.2027.
20. Duthie, S. J. (1999) Folic acid deficiency and cancer: Mechanisms of DNA instability. *Br. Med. Bull.* **55**, 578–592. https://doi.org/10.1258/0007142991902646.
21. Pieroth, R., Paver, S., Day, S. and Lammersfeld, C. (2018) Folate and its impact on cancer risk. *Curr. Nutr. Rep.* **7**, 70–84. https://doi.org/10.1007/s13668-018-0237-y.

22. Lowry, O. H., Bessey, O. A. and Crawford, E. J. (1949) Photolytic and enzymatic transformations of pteroylglutamic acid. *J. Biol. Chem.* **180**, 389–398.

23. Jamil Akhtar, M., Ataullah Khan, M. and Ahmad, I. (2003) Identification of photoproducts of folic acid and its degradation pathways in aqueous solution. *J. Pharm. Biomed. Anal.* **31**, 579–588. https://doi.org/10.1016/S0731-7085(02)00724-0.

24. Thomas, A. H., Suárez, G., Cabrerizo, F. M., Martino, R. and Capparelli, A. L. (2000) Study of the photolysis of folic acid and 6-formylpterin in acid aqueous solutions. *J. Photochem. Photobiol. A Chem.* **135**, 147–154.

25. Dántola, M. L., Denofrio, M. P., Zurbano, B., Gimenez, C. S., Ogilby, P. R., Lorente, C. and Thomas, A. H. (2010) Mechanism of photooxidation of folic acid sensitized by unconjugated pterins. *Photochem. Photobiol. Sci.* **9**, 1604–1612.

26. Goossens, J.-F., Thuru, X. and Bailly, C. (2021) Properties and reactivity of the folic acid and folate photoproduct 6-formylpterin. *Free Radic. Biol. Med.* **171**, 1–10. https://doi.org/https://doi.org/10.1016/j.freeradbiomed.2021.05.002.

27. Petroselli, G., Dántola, M. L., Cabrerizo, F. M., Capparelli, A. L., Lorente, C., Oliveros, E. and Thomas, A. H. (2008) Oxidation of 2'-deoxyguanosine 5'-monophosphate photoinduced by pterin: Type I versus type II mechanism. *J. Am. Chem. Soc.* **130**, 3001–3011.

28. Serrano, M. P., Vignoni, M., Lorente, C., Vicendo, P., Oliveros, E. and Thomas, A. H. (2016) Thymidine radical formation via one-electron transfer oxidation photoinduced by pterin: Mechanism and products characterization. *Free Radic. Biol. Med.* **96**, 418–431. https://doi.org/10.1016/j.freeradbiomed.2016.04.196.

29. Castaño, C., Vignoni, M., Vicendo, P., Oliveros, E. and Thomas, A. H. (2016) Degradation of tyrosine and tryptophan residues of peptides by type I photosensitized oxidation. *J. Photochem. Photobiol. B Biol.* **164**, 226–235.

https://doi.org/10.1016/j.jphotobiol.2016.09.024.
30. Reid, L. O., Dántola, M. L., Petroselli, G., Erra-Balsells, R., Miranda, M. A., Lhiaubet-Vallet, V. and Thomas, A. H. (2019) Chemical modifications of globular proteins phototriggered by an endogenous photosensitizer. *Chem. Res. Toxicol.* **32**, 2250–2259. https://doi.org/10.1021/acs.chemrestox.9b00286.
31. Dantola, M. L., Reid, L. O., Castaño, C., Lorente, C., Oliveros, E. and Thomas, A. H. (2017) Photosensitization of peptides and proteins by pterin derivatives. *Pteridines* **28**, 105–114.
32. Denofrio, M. P., Lorente, C., Breitenbach, T., Hatz, S., Cabrerizo, F. M., Thomas, A. H. and Ogilby, P. R. (2011) Photodynamic effects of pterin on HeLa cells. *Photochem. Photobiol.* **87**, 862–866.
33. Thomas, A. H., Catalá, Á. and Vignoni, M. (2016) Soybean phosphatidylcholine liposomes as model membranes to study lipid peroxidation photoinduced by pterin. *Biochim. Biophys. Acta - Biomembr.* **1858**, 139–145. https://doi.org/10.1016/j.bbamem.2015.11.002.
34. Walalawela, N., Urrutia, M. N., Thomas, A. H., Greer, A. and Vignoni, M. (2019) Alkane chain-extended pterin through a pendent carboxylic acid acts as triple functioning fluorophore, 1O2 sensitizer and membrane binder. *Photochem. Photobiol.* **95**, 1160–1168. https://doi.org/10.1111/php.13098.
35. Ghosh, G., Belh, S. J., Chiemezie, C., Walalawela, N., Ghogare, A. A., Vignoni, M., Thomas, A. H., McFarland, S. A., Greer, E. M. and Greer, A. (2019) S,S-Chiral linker induced U shape with a Syn-facial sensitizer and photocleavable ethene group. *Photochem. Photobiol.* **95**, 293–305. https://doi.org/10.1111/php.13000.
36. Kimani, S., Ghosh, G., Ghogare, A., Rudshteyn, B., Bartusik, D., Hasan, T. and Greer, A. (2012) Synthesis and characterization of mono-, Di-, and tri-poly(ethylene

glycol) chlorin e6 conjugates for the photokilling of human ovarian cancer cells. *J. Org. Chem.* **77**, 10638–10647. https://doi.org/10.1021/jo301889s.

37. Hamblin, M., Miller, J. L., Rizvi, I., Ortel, B., Maytin, E. V and Hasan, T. (2001) Pegylation of a chlorin(e6) polymer conjugate increases tumor targeting of photosensitizer. *Cancer Res.* **61**, 7155–7162.

38. Kuhn, H. J., Braslavsky, S. E. and Schmidt, R. (2004) Chemical actinometry (IUPAC technical report). *Pure Appl. Chem.* **76**, 2105–2146.

39. Allain, C. C., Poon, L. S., Chan, C. S. G., Richmond, W. and Fu, P. C. (1974) Enzymatic determination of total serum cholesterol. *Clin. Chem.* **20**, 470–475.

40. Flegg, H. M. (1973) An investigation of the determination of serum cholesterol by an enzymatic method. *Ann. Clin. Biochem.* **10**, 79–84.

41. Frisch, M. J., Trucks, G. W., Schlegel, H. B., Scuseria, G. E., Robb, M. A., Cheeseman, J. R., Scalmani, G., Barone, V., Petersson, G. A., Nakatsuji, H., Li, X., Caricato, M., Marenich, A. V., Bloino, J., Janesko, B. G., Gomperts, R., Mennucci, B., Hratchian, H. P., Ortiz, J. V., Izmaylov, A. F., Sonnenberg, J. L., Williams-Young, D., Ding, F., Lipparini, F., Egidi, F., Goings, J., Peng, B., Petrone, A., Henderson, T., Ranasinghe, D., Zakrzewski, V. G., Gao, J., Rega, N., Zheng, G., Liang, W., Hada, M., Ehara, M., Toyota, K., Fukuda, R., Hasegawa, J., Ishida, M., Nakajima, T., Honda, Y., Kitao, O., Nakai, H., Vreven, T., Throssell, K., Montgomery, J. A. J., Peralta, J. E., Ogliaro, F., Bearpark, M. J., Heyd, J. J., Brothers, E. N., Kudin, K. N., Staroverov, V. N., Keith, T. A., Kobayashi, R., Normand, J., Raghavachari, K., Rendell, A. P., Burant, J. C., Iyengar, S. S., Tomasi, J., Cossi, M., Millam, J. M., Klene, M., Adamo, C., Cammi, R., Ochterski, J. W., Martin, R. L., Morokuma, K., Farkas, O., Foresman, J. B. and Fox, D. J. (2016) Gaussian 16, Revision C.01.

42. Walalawela, N., Vignoni, M., Urrutia, M. N., Belh, S. J., Greer, E. M., Thomas, A.

H. and Greer, A. (2018) Kinetic control in the regioselective alkylation of pterin sensitizers: A synthetic, photochemical, and theoretical study. *Photochem. Photobiol.* **94**, 834–844. https://doi.org/10.1111/php.12905.

43. Szakács, Z. and Noszál, B. (2006) Determination of dissociation constants of folic acid, methotrexate, and other photolabile pteridines by pressure-assisted capillary electrophoresis. *Electrophoresis* **27**, 3399–3409. https://doi.org/10.1002/elps.200600128.

44. Cabrerizo, F. M., Petroselli, G., Lorente, C., Capparelli, A. L., Thomas, A. H., Braun, A. M. and Oliveros, E. (2005) Substituent effects on the photophysical properties of pterin derivatives in acidic and alkaline aqueous solutions. *Photochem. Photobiol.* **81**, 1234–1240.

45. Li, G., Magana, D. and Dyer, R. B. (2012) Photoinduced electron transfer in folic acid investigated by ultrafast infrared spectroscopy. *J. Phys. Chem. B* **116**, 3467–3475. https://doi.org/10.1021/jp300392a.

46. Suárez, G., Cabrerizo, F. M., Lorente, C., Thomas, A. H. and Capparelli, A. L. (2000) Study of the photolysis of 6-carboxypterin in acid and alkaline aqueous solutions. *J. Photochem. Photobiol. A Chem.* **132**, 53–57.

47. Dántola, M. L., Vignoni, M., González, C., Lorente, C., Vicendo, P., Oliveros, E. and Thomas, A. H. (2010) Electron-transfer processes induced by the triplet state of pterins in aqueous solutions. *Free Radic. Biol. Med.* **49**, 1014–1022.

48. Leamon, C. P. and Low, P. S. (1991) Delivery of macromolecules into living cells: A method that exploits folate receptor endocytosis. *Proc. Natl. Acad. Sci. U. S. A.* **88**, 5572–5576. https://doi.org/10.1073/pnas.88.13.5572.

49. Antony, A. C. (1996) Folate receptors. *Annu. Rev. Nutr.* **16**, 501–521. https://doi.org/10.1146/annurev.nu.16.070196.002441.

50. Ross, J. F., Chaudhuri, P. K. and Ratnam, M. (1994) Differential regulation of folate receptor isoforms in normal and malignant tissues in vivo and in established. *Cancer* **73**, 2432–2443.

51. Weitman, S. D., Weinberg, A. G., Coney, L. R., Zurawski, V. R., Jennings, D. S. and Kamen, B. A. (1992) Cellular localization of the folate receptor: potential role in drug toxicity and folate homeostasis. *Cancer Res.* **52**, 6708–6711.

52. Leamon, C. P. and Low, P. S. (1992) Cytotoxicity of momordin-folate conjugates in cultured human cells. *J. Biol. Chem.* **267**, 24966–24971. https://doi.org/10.1016/s0021-9258(19)73992-1.

53. Vlahov, I. R., Santhapuram, H. K. R., Kleindl, P. J., Howard, S. J., Stanford, K. M. and Leamon, C. P. (2006) Design and regioselective synthesis of a new generation of targeted chemotherapeutics. Part 1: EC145, a folic acid conjugate of desacetylvinblastine monohydrazide. *Bioorganic Med. Chem. Lett.* **16**, 5093–5096. https://doi.org/10.1016/j.bmcl.2006.07.030.

54. Bellotti, E., Cascone, M. G., Barbani, N., Rossin, D., Rastaldo, R., Giachino, C. and Cristallini, C. (2021) Targeting cancer cells overexpressing folate receptors with new terpolymer-based nanocapsules: Toward a novel targeted dna delivery system for cancer therapy. *Biomedicines* **9**. https://doi.org/10.3390/biomedicines9091275.

55. Chen, C., Ke, J., Edward Zhou, X., Yi, W., Brunzelle, J. S., Li, J., Yong, E. L., Xu, H. E. and Melcher, K. (2013) Structural basis for molecular recognition of folic acid by folate receptors. *Nature* **500**, 486–489. https://doi.org/10.1038/nature12327.

FIGURE CAPTIONS

Figure 1. Chemical structure of pteroic acid (Pte) and folic acid or pteroyl glutamic acid (PteGlu).

Scheme 1. Synthesis of *bis*-decyl-Pte.

Figure 2. Partial 2D NMR spectra of *bis*-decyl-Pte recorded in $CDCl_3$, using HMBC method.

Figure 3. B3LYP/D95(d,p) computed minimum free energy structures (ΔG) of *mono*-decylated pteroic acid derivatives. Free energies are shown in kcal/mol.

Figure 4. B3LYP/D95(d,p) computed minimum free energy structures (ΔG) of *bis*-decylated pteroic acid derivatives. Free energies are shown in kcal/mol.

Figure 5. B3LYP/D95(d,p) computed minimum free energy structures (ΔG) of *tris*-decylated pteroic acid derivatives. Free energies are shown in kcal/mol.

Figure 6. Absorption spectra of a) Pte in aqueous solution at different pH and b) *bis*-decyl-Pte in MeOH.

Figure 7. Time evolution of concentrations of Pte and products (PABA, Fop, Cap and Ptr) in air-equilibrated aqueous solutions under UVA irradiation. $[Pte]_0 = 25$ μM, pH = 6.7. Inset: Time evolution of H_2O_2 generated during the mentioned experiment.

Scheme 2. Proposed mechanism for the photooxidative cleavage of Pte and *bis*-decyl-Pte in air-equilibrated aqueous (pH = 6.7) and MeOH/H_2O solutions, respectively, under UVA irradiation, followed by decomposition of the photoproducts. Ptr was observed only in the photocleavage of Pte.

Figure 8. Time evolution of % consumption of Pte in H_2O and *bis*-decyl-Pte in MeOH and MeOH/H_2O solutions under UVA irradiation. $[Pte]_0 = 25$ μM and [*bis*-decyl-Pte]$_0$ = 27 μM.

Figure 9. Chromatogram of *bis*-decyl-Pte in MeOH/H_2O solution after 30 min of irradiation using the PDA detector at 310 nm. Upper/bottom part: Absorption spectra of the different chromatographic peaks, *bis*-decyl-Pte and products 1 to 5.

Figure 10. Elution profiles of size exclusion chromatography performed on DOPC LUVs with *bis*-decyl-Pte. For each fraction absorbance at 600 nm (●) and the area at 340 nm for the compound obtained from the chromatogram (●) were registered to detect the LUVs and *bis*-decyl-Pte, respectively.

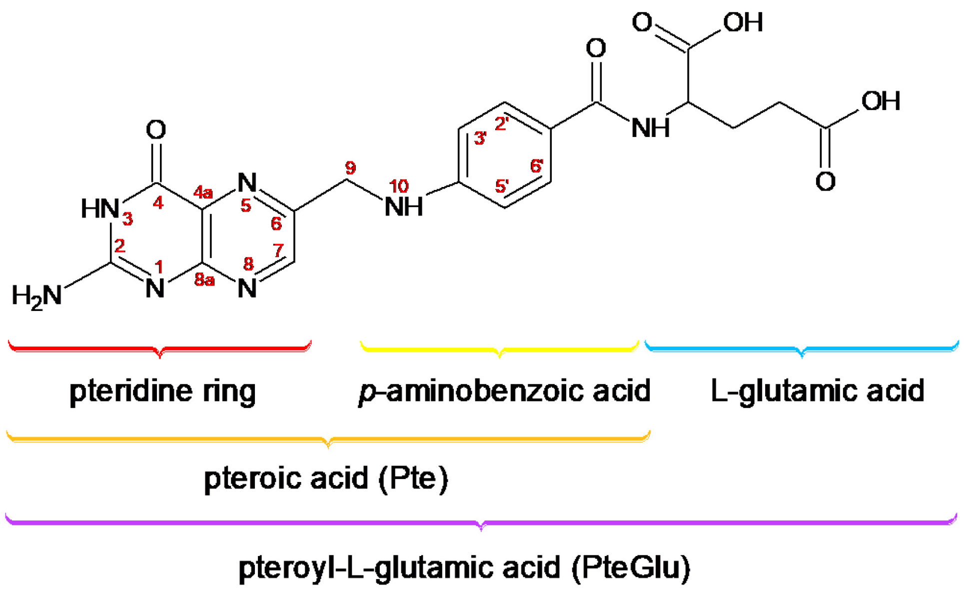

Figure 1. Chemical structure of pteroic acid (Pte) and folic acid or pteroyl glutamic acid (PteGlu).

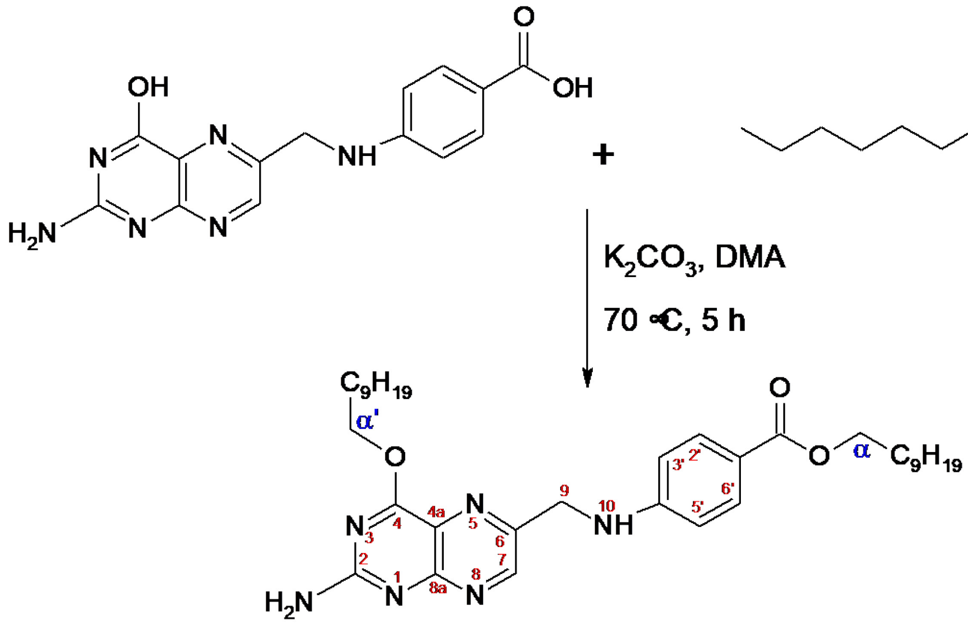

Scheme 1. Synthesis of *bis*-decyl-Pte.

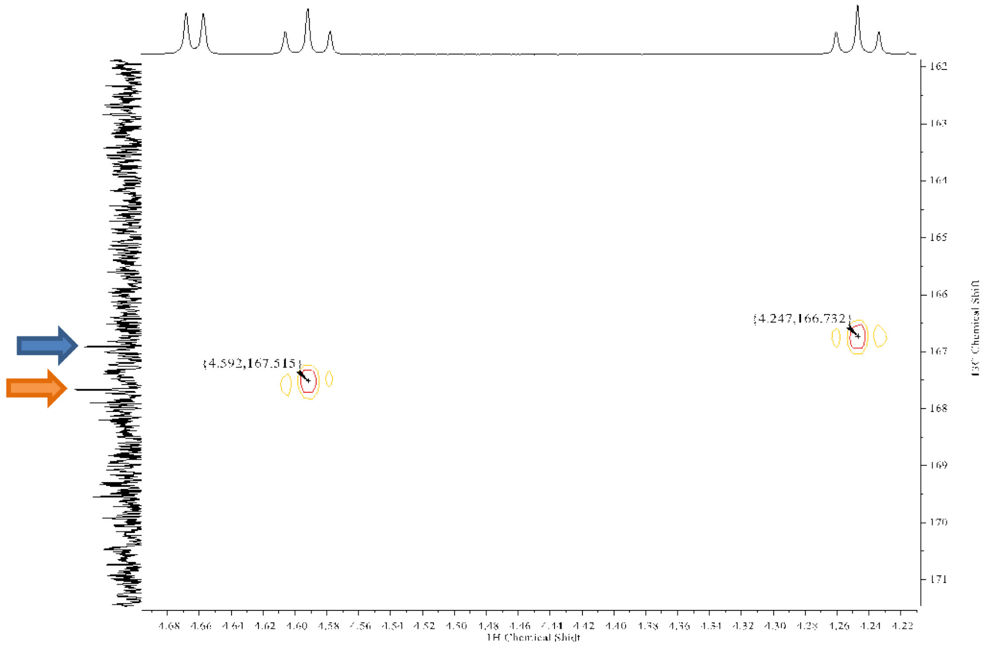

Figure 2. Partial 2D NMR spectra of *bis*-decyl-Pte recorded in $CDCl_3$, using HMBC method.

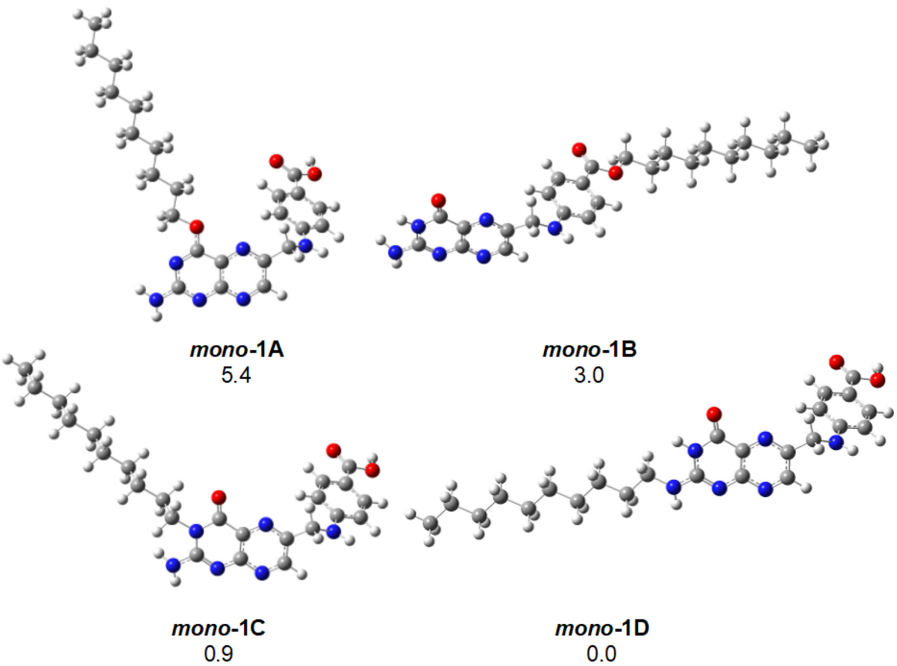

Figure 3. B3LYP/D95(d,p) computed minimum free energy structures (Δ*G*) of *mono*-decylated pteroic acid derivatives. Free energies are shown in kcal/mol.

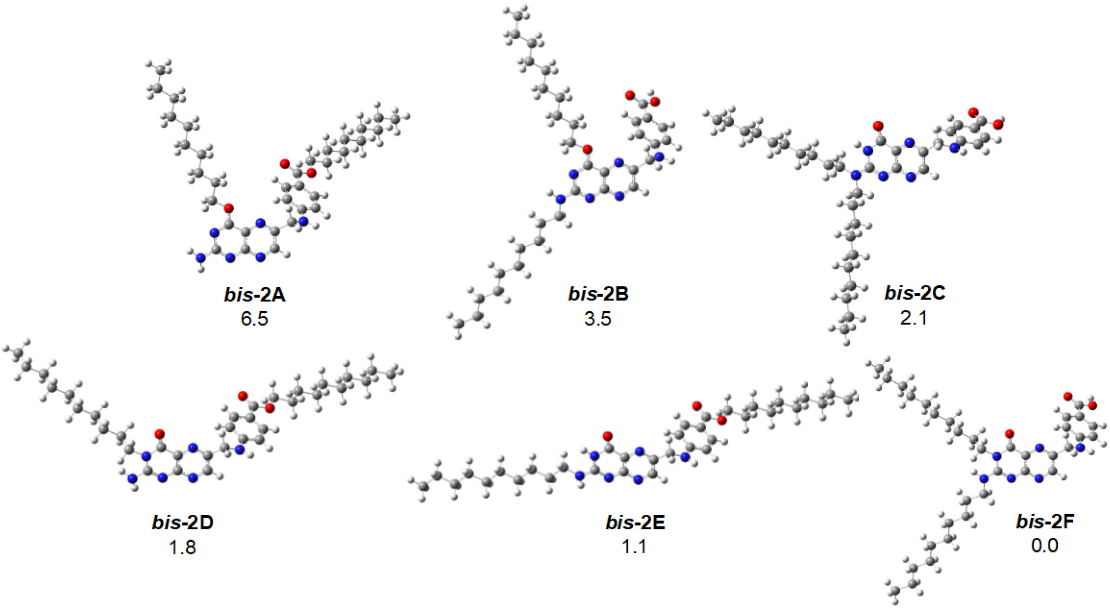

Figure 4. B3LYP/D95(d,p) computed minimum free energy structures (Δ*G*) of *bis*-decylated pteroic acid derivatives. Free energies are shown in kcal/mol.

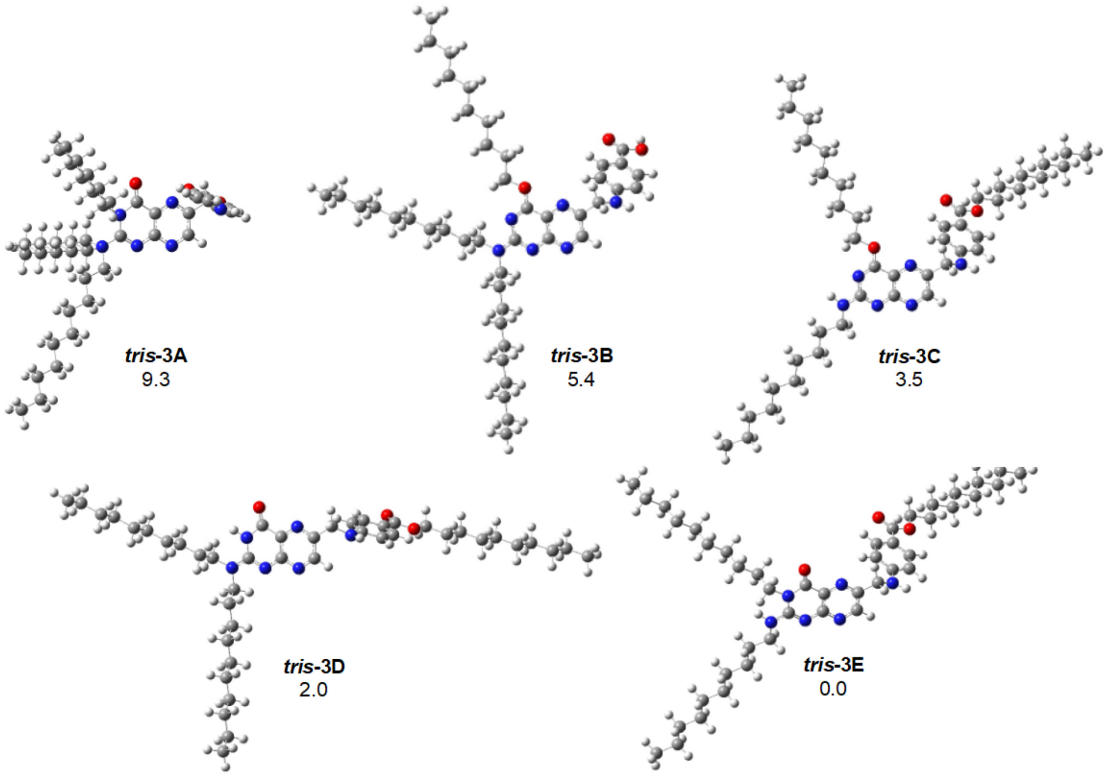

Figure 5. B3LYP/D95(d,p) computed minimum free energy structures (Δ*G*) of *tris*-decylated pteroic acid derivatives. Free energies are shown in kcal/mol.

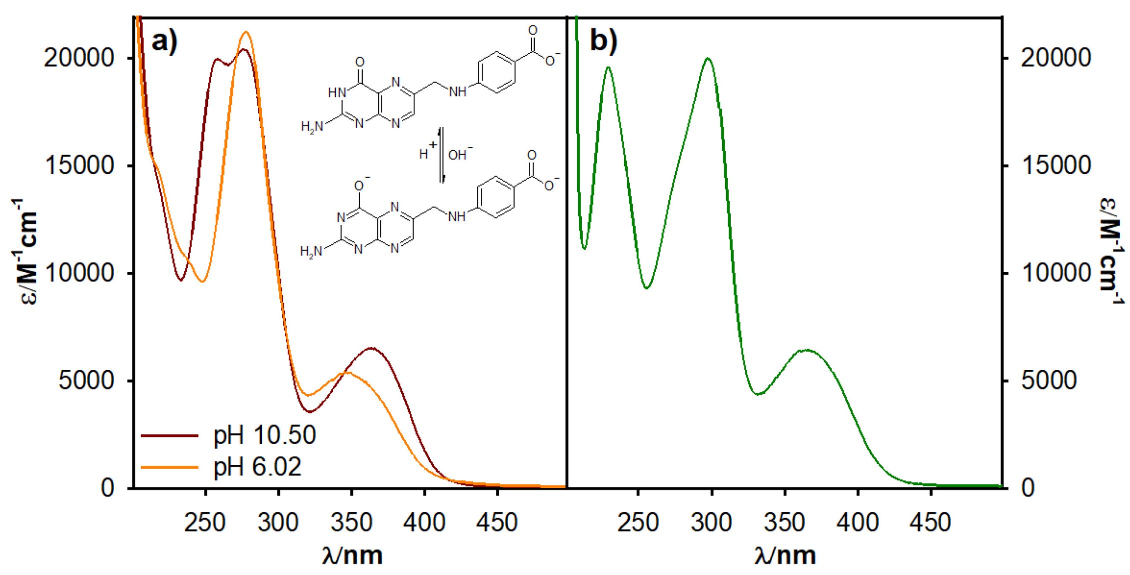

Figure 6. Absorption spectra of a) Pte in aqueous solution at different pH and b) *bis*-decyl-Pte in MeOH.

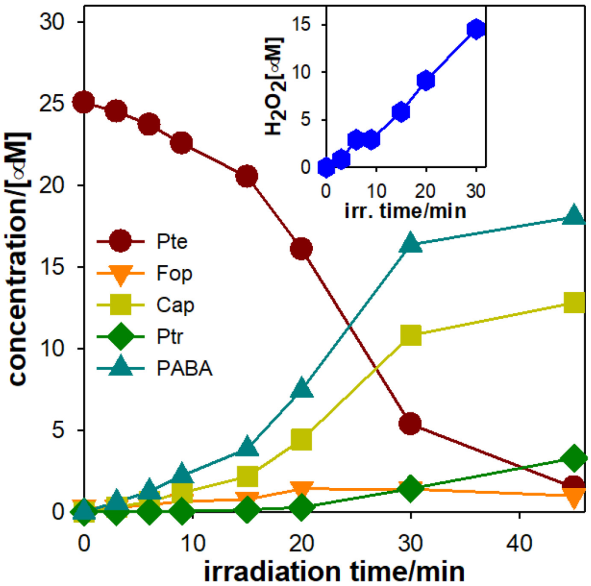

Figure 7. Time evolution of concentrations of Pte and products (PABA, Fop, Cap and Ptr) in air-equilibrated aqueous solutions under UVA irradiation. $[Pte]_0$ = 25 µM, pH = 6.7. Inset: Time evolution of H_2O_2 generated during the mentioned experiment.

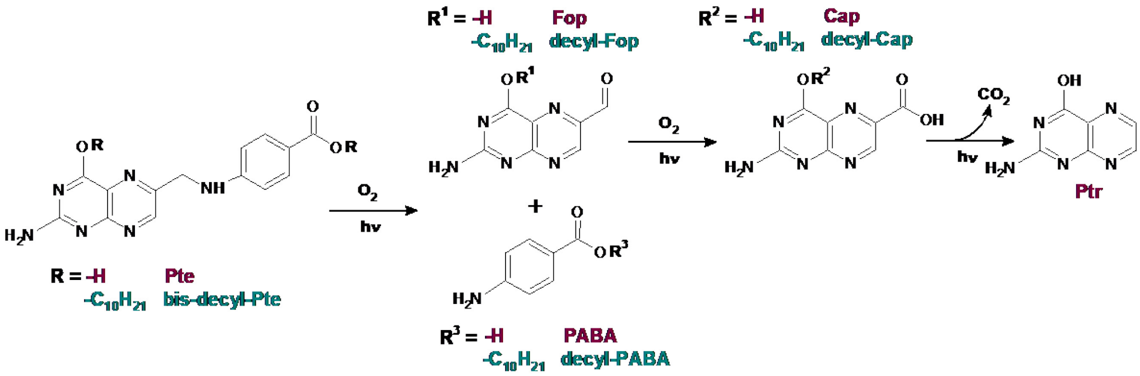

Scheme 2. Proposed mechanism for the photooxidative cleavage of Pte and *bis*-decyl-Pte in air-equilibrated aqueous (pH = 6.7) and MeOH/H_2O solutions, respectively, under UVA irradiation, followed by decomposition of the photoproducts. Ptr was observed only in the photocleavage of Pte.

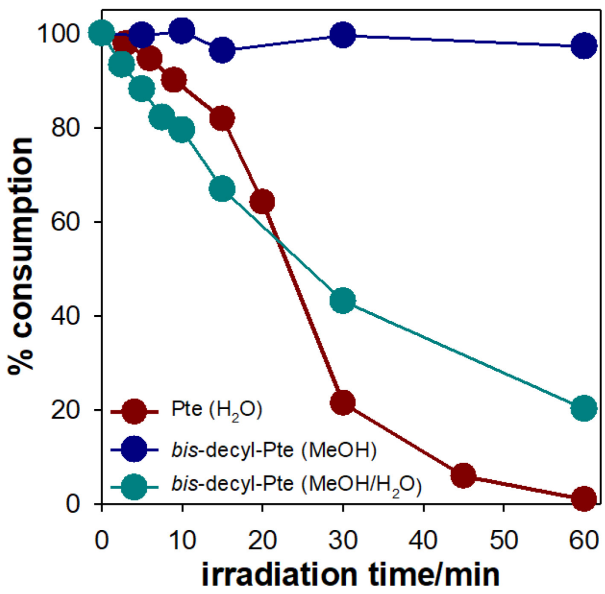

Figure 8. Time evolution of % consumption of Pte in H_2O and *bis*-decyl-Pte in MeOH and MeOH/H_2O solutions under UVA irradiation. $[Pte]_0$ = 25 µM and [*bis*-decyl-Pte]$_0$ = 27 µM.

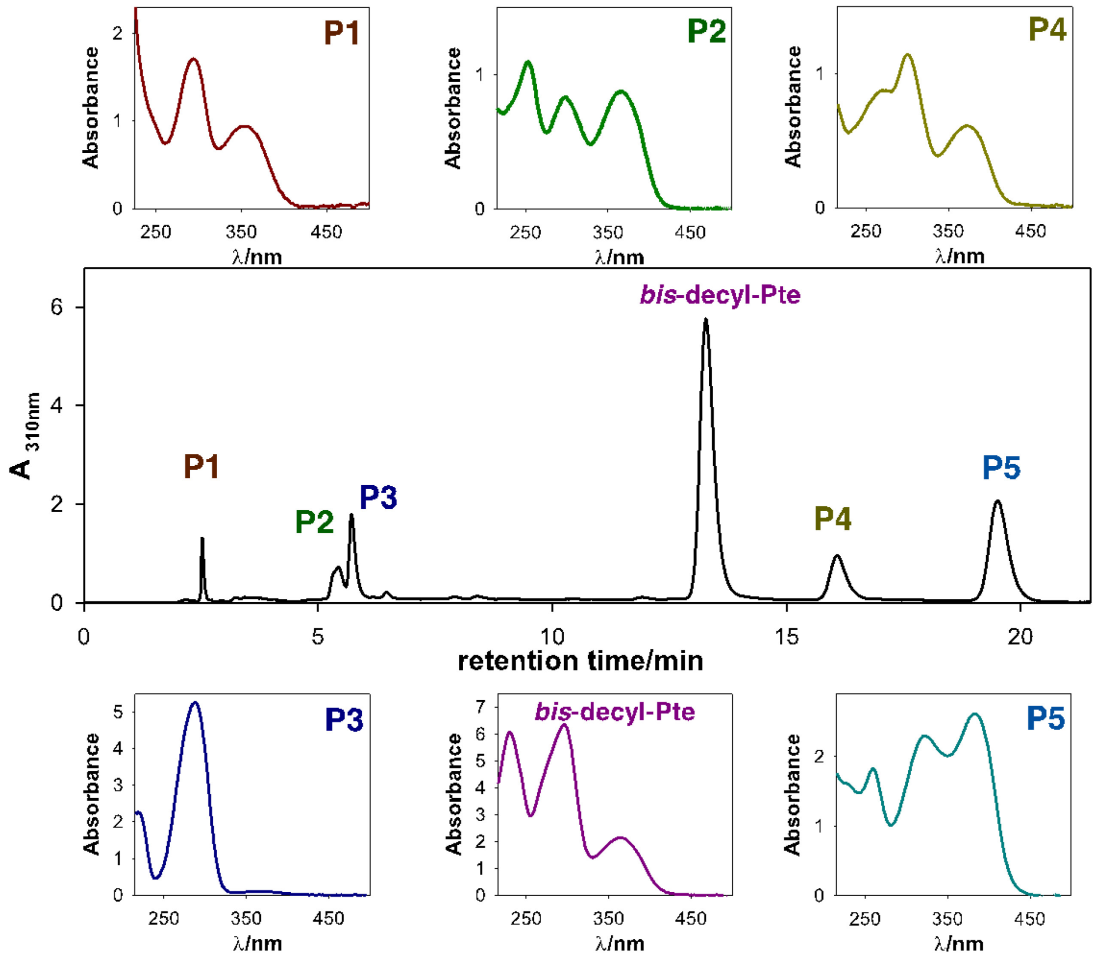

Figure 9. Chromatogram of *bis*-decyl-Pte in MeOH/H_2O solution after 30 min of irradiation using the PDA detector at 310 nm. Upper/bottom part: Absorption spectra of the different chromatographic peaks, *bis*-decyl-Pte and products 1 to 5.

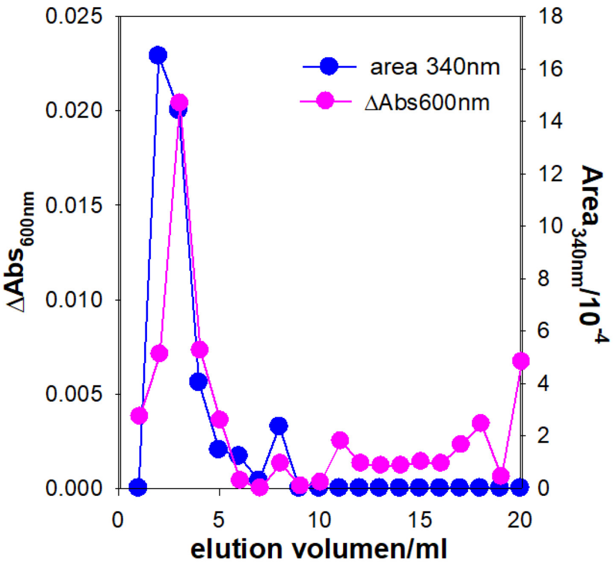

Figure 10. Elution profiles of size exclusion chromatography performed on DOPC LUVs with *bis*-decyl-Pte. For each fraction absorbance at 600 nm (●) and the area at 340 nm for the compound obtained from the chromatogram (●) were registered to detect the LUVs and *bis*-decyl-Pte, respectively.